https://doi.org/10.1016/j.apr.2024.102383

Advancing Urban Air Quality Modeling with Solar Radiation-included Computational Fluid Dynamics Simulations

Nicolas Reiminger[1,2,†], Xavier Jurado[1], Loïc Maurer[3], José Vazquez[3], Cédric Wemmert[2]

[1]AIR&D, 32 rue Wimpheling, F-67000, Strasbourg, France
[2]ICube Laboratory, UMR 7357, CNRS/University of Strasbourg, F-67000, Strasbourg, France
[3]Université de Strasbourg, CNRS, ENGEES, ICube UMR 7357, Département Mécanique, F-67000, Strasbourg, France

[†] Corresponding author: Tel. +33 (0)6 31 26 75 88, Mail. nreiminger@air-d.fr

Citation : Reiminger, N., Jurado, X., Maurer, L., Vazquez, J., & Wemmert, C. (2025). Advancing urban air quality modeling with solar radiation-included computational fluid dynamics simulations. Atmospheric Pollution Research, 16(2), 102383. https://doi.org/10.1016/j.apr.2024.102383

Abstract

Air quality modeling is a challenging task due to the complex interactions among meteorological, chemical, and physical processes. Accurate predictions require sophisticated models that can simulate these interactions under varying environmental conditions. This study advances micro-scale urban air quality modeling knowledge by considering solar radiation-included Computational Fluid Dynamics (CFD) simulations. Using data on air pollution concentration monitored in Antwerp, Belgium, this research evaluates the benefits of incorporating non-isothermal conditions and solar radiation into CFD air pollution dispersion models compared to the traditional neutral boundary layer assumption. The study analyzes twelve hourly meteorological case studies under non-isothermal conditions with solar radiation included to assess the accuracy and performance of both approaches. Findings reveal that the non-neutral CFD model outperforms the neutral model in 75% of the scenarios, with differences in the concentration maps ranging from 8% to 32%. These disparities significantly affect the identification of concentration hotspots and pollutant level predictions. Accuracy assessments against in-field monitored data show notable reductions in relative errors for the non-neutral model, averaging 21%, compared to 40% for the neutral model. While both models perform similarly under low wind speed and low solar radiation conditions, the non-neutral model generally demonstrates superior performance under higher solar radiation and more variable wind speeds. Overall, the non-neutral model offers an improvement factor of around 2 compared to the neutral model. The integration of solar radiation in CFD simulations represents a significant advancement in urban air quality modeling, with promising implications for enhancing air quality management and urban planning decisions.

Keywords: CFD, air quality, urban area, solar radiation, thermal effects

1. Introduction

Air pollution has become a significant issue in recent decades (Manisalidis et al., 2020), consequently becoming a prominent challenge for modern societies (Agathokleous and Sicard, 2021). In urban areas, air quality can be particularly poor due to a lot of anthropogenic sources of air pollutants such as traffic-related emissions and residential heating (Thunis, 2018). On the meantime, people are increasingly living in such places (United Nations, 2019), which exacerbates both the problems of anthropogenic emissions as well as the number of people exposed to air pollution (Chen et al., 2017). To face this issue, European cities have taken various actions to improve air quality with the aim of protecting human health and improving the well-being of their citizens (Viana et al., 2020). However, local air pollution mitigation measures can also be counterproductive (Santiago et al., 2024) and, despite significant progress, many European cities still exceed European Union (EU) and World Health Organization (WHO) air quality standards (EEA, 2023). It is therefore essential to be able to define effective planning strategies to improve air quality (Rodrigues et al., 2021) and to test them at an early stage to ensure their effectiveness.

Numerical modeling is a valuable tool for such purpose (O'Regan and Nyhan, 2023). Among the many different types of models available, each adapted to specific spatial and temporal scales (Toparlar et al.,

2017), computational fluid dynamics (CFD) models have shown a strong interest for modeling air quality in urban areas (Pantusheva et al., 2022). Indeed, urban infrastructures and their morphological characteristics have a significant impact on air pollution dispersion (Badach et al., 2023; Tian et al., 2019), a point that is explicitly accounted for by computational fluid dynamics (CFD) models. Such model is, therefore, highly suitable for modeling the precise effects of street canyons (Hang et al., 2022; Sin et al., 2023) and other civil engineering structures (Choi et al., 2023; Ming et al., 2023) on wind distribution, thus, on air pollution dispersion. Besides, CFD models also allow many specific phenomena to be considered and modeled, such as the effects of vegetation on wind flow and air pollutant concentration (Guo et al., 2023; Wang et al., 2023), as well as the influence of the traffic on pollutant dispersion (Zheng and Yang, 2022, 2021). Despite this, CFD models are mostly used to study idealized cases in order to characterize the influence of specific parameters on pollutant dispersion, rather than in applied air quality contexts (Pantusheva et al., 2022). Recent work comparing eleven CFD models to one Lagrangian, three Gaussian and one artificial intelligence (AI) models against in situ experimental data has nevertheless shown the value of CFD models in assessing real urban air quality. Indeed, authors have shown that such a model outperforms the other types of models, particularly the Gaussian ones, which tend to underestimate concentration gradients (Martín et al., 2024). Their findings align with the results of the European action COST ES 1006, which comprehensively evaluated the performance and capabilities of various modeling approaches—ranging from simple Gaussian models to advanced CFD models—in predicting air quality within the built environment (Baumann-Stanzer et al., 2015).

In this way, CFD modeling is a key tool for simulating air quality in urban areas under real and uncontrolled conditions. However, in contrast to other conventionally used models such as Gaussian ones, it is common in real-context urban CFD simulations to assume isothermal conditions (i.e., neutral boundary layer conditions) rather than including non-isothermal ones. While non-isothermal conditions are often studied in idealized simulations, their incorporation in real-context scenarios remains less frequent due to the computational complexity involved (Reiminger et al., 2024). This assumption can yield good results when several simulations are combined to obtain averaged monthly pollutant concentrations (Martín et al., 2024), but this result may depend on the case studied. Errors and misleading interpretations could also be made if the results were studied one by one, on an hourly basis for instance. Indeed, studies have shown that non-isothermal conditions, and particularly unstable thermal conditions, significantly affect airflow and ventilation in urban street canyon (Chen et al., 2023) as well as the dispersion of air pollutants (Guo et al., 2023). Such studies provide valuable information on the influence of heat transfer on air pollution dispersion. However, they are also usually based on strong assumptions, such as setting constant hypothetical temperatures on building facades. In practice, constant temperatures are rarely observed on entire facades of buildings, as a given facade of a building may be partly sunny and partly shaded at the same time, depending on the position of the sun and the surrounding buildings. This point also applies to horizontal surfaces, such as roofs or the ground. The latter issue also considerably modifies the dispersion of atmospheric pollutants (Kubilay et al., 2018). Therefore, further research is required to evaluate the benefits of incorporating non-isothermal conditions and solar radiation into micro-scale modeling of air pollution dispersion in real urban areas, which is the focus of the present work.

The aim of this study is to compare the results obtained by two CFD air quality models with data measured in a real urban environment limited to diurnal summertime meteorological cases. In particular, the two models considered correspond to CFD models with (1) the usual assumption of a neutral boundary layer condition (no thermal effects) and (2) considering thermal effects, surface temperatures and shadows modeled by a solar radiative model. To achieve this objective, several CFD simulations were performed in two districts of the city of Antwerp, Belgium, considering real hourly meteorological conditions observed during daytime (including wind direction and speed, air temperature, solar radiation, and time). The concentrations obtained by the two CFD models were first compared with each other, before being compared with hourly NO_2 concentrations measured by a local air quality monitoring station. All the details about the study location, data availability and information about the numerical model are described in Section 2. Results are presented in Section 3 before being discussed in Section 4. Lastly, conclusions and perspectives of this work are drawn in Section 5.

2. Material and methods

2.1. Study location and data availability

The study was conducted in the city of Antwerp, Belgium, in an area running through the Borgerhout and Zurenborg districts (from 51.2083, 4.4279 to 51.2118, 4.4347 GPS coordinates). This densely built-up area, characteristic of the cities of Western Europe, primarily consists of two- to three-storey commercial and residential building, forming street canyons. Large open areas are also present, consisting of car parks and green areas. Although there are no major industrial sources of air pollution in the studied area, numerous sources of air pollutants from traffic are present, notably the N184 national road. Lastly, an air quality (AQ) station operated by the Flemish Environment Agency (VMM) is located in the center of the area along the N184. The exact location of the area of interest is given in **Figure 1**, which also indicates the AQ station location.

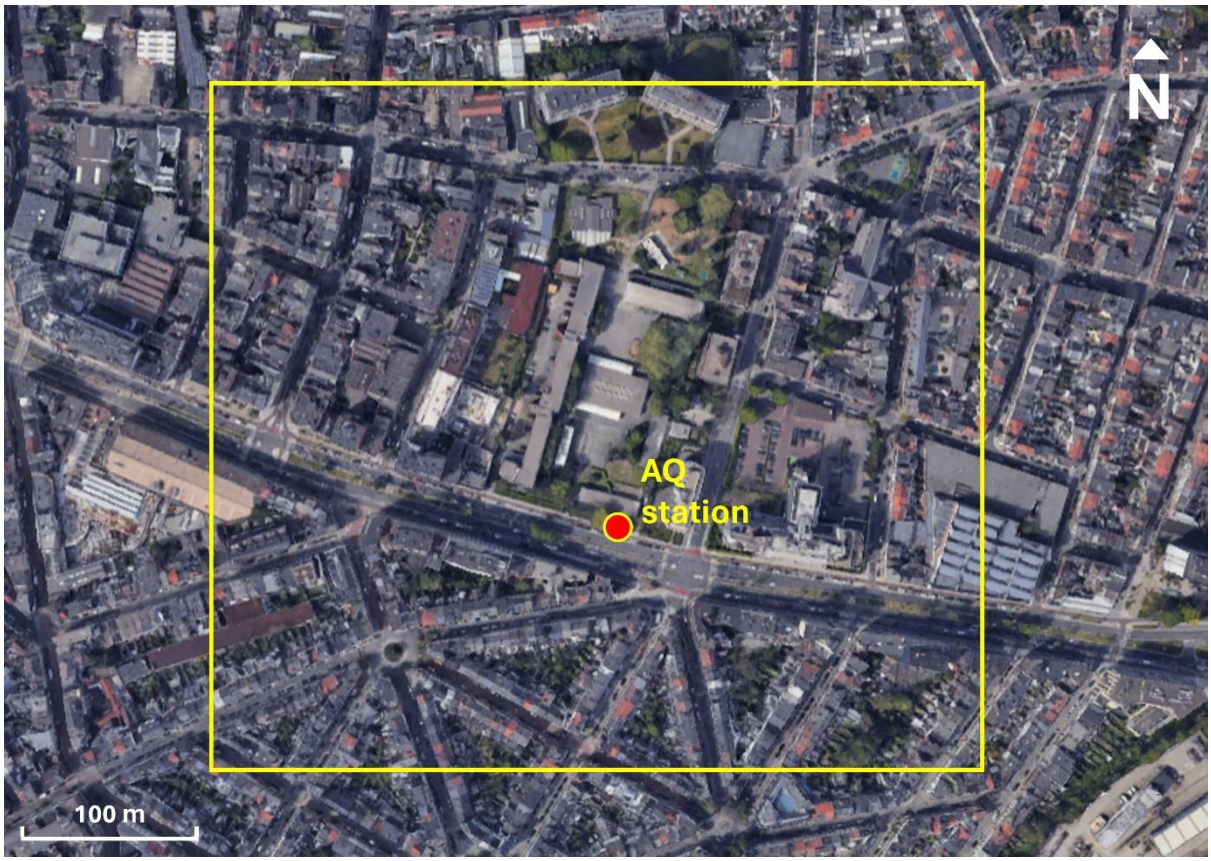

Figure 1. Satellite map showing the study area boundaries (yellow rectangle) and locating the air quality (AQ) station location (red circle).

All input data used in this study were provided by the FAIRMODE (Forum for Air Quality Modeling in Europe) community. Detailed information about these data can be found in Martín et al. (2024). In summary, the available data include:

- **Buildings and roads layout**: 3D LOD1 (level of detail 1) data corresponding to 2D sketches (with associated heights for the building), acquired from the 3D GRB Informatic Vlaanderen and available on their website (https://overheid.vlaanderen.be/grb-3dgrb).

- **Meteorological data**: corresponding to hourly information of averaged wind direction, wind velocity, temperature, total solar radiation and humidity monitored throughout 2016 at the Antwerp-Luchtbal measurement station (5 km north of the studied area, coordinates: 51.261, 4.425). Although a station located within the city center would have been preferable to better capture urban microclimatic conditions, the Antwerp-Luchtbal station was the nearest meteorological station available.

- **Emission data**: corresponding to traffic-related emission of nitrogen oxides (NO_x), nitrogen dioxide (NO_2), black carbon (BC) and particulate matters (PM10 and PM2.5) obtained using the Fastrace Traffic Model v2.1 (Hooyberghs et al., 2022). These data consider the official 2016 traffic and fleet data from the Department for Mobility and is based on the COPERT 5 emission factors.

- **Background air pollution concentrations**: corresponding to hourly concentrations of nitric oxide (NO), ozone (O_3), NO_2, BC, PM10 and PM2.5 obtained by the VITO (Flemish Institute for Technological Research), using the RIO model (Janssen et al., 2008).

Lastly, while numerous pollutants are available in the data collection, this work is limited to the study of nitrogen dioxide (NO_2) concentrations.

2.2. Numerical model

2.2.1. Software and calculation methodology

All the simulations were performed through the OpenFOAM v2306 CFD software (https://www.openfoam.com/news/main-news/openfoam-v2306), working in parallel calculation on a 32-core Intel® Xeon(R) Silver 4216 CPU E5–2670 2.10 GHz computing machine under Ubuntu 20.04.5 LTS.

The CFD solver used in this study is the *buoyantBoussinesqPimpleFoam* solver, a transient mixed convection solver from the OpenFOAM library able of reproducing both forced and natural convection. In particular, this solver solves the incompressible Navier-Stokes equations including turbulent- but also buoyancy-driven flows by considering the Boussinesq approximation. Note that this approximation, well known for simplifying physics problems and often used in wind engineering and air pollution assessment (Ghobadi and Nasrollahi, 2021; Liu et al., 2021), only introduces errors of the order of 1% if the temperature differences between extreme values are below 15 K for air (Ferziger and Perić, 2002).

An Unsteady Reynolds-Averaged Navier-Stokes (URANS) methodology was chosen to solve the Navier-Stokes equations, as it provides better, or at least equivalent results compared to steady-state calculations (Tominaga and Stathopoulos, 2017). The RNG k-epsilon turbulent closure scheme is used to solve the Reynolds stress tensor arising when using the RANS methodology, this closure scheme leading to good results for urban air pollution dispersion modeling through CFD RANS in a real urban context (Reiminger et al., 2024).

The native *buoyantBoussinesqPimpleFoam* solver from the OpenFOAM library has been slightly modified to account for pollutant dispersion by implementing the turbulent advection-diffusion equation **(1)** governing passive scalar transport:

$$\frac{\partial C}{\partial t} + \nabla.(Cu) - \nabla.\left[\left(D_m + \frac{\nu_t}{Sc_t}\right)\nabla C\right] = E \qquad (1)$$

where C is the pollutant concentration [g.m^{-3}], t is the time [s], u is the velocity [m.s^{-1}], D_m is the molecular diffusion coefficient [m^{-2}.s^{-1}], ν_t is the turbulent diffusivity [m^{-2}.s^{-1}], Sc_t is the turbulent Schmidt number set to 0.7 [-] and E is the emission of pollutants [g.s^{-1}].

Given that the numerical solver does not account for any chemical mechanism and that the pollutant of interest in this study is nitrogen dioxides (NO_2), the empirical function of Bächlin et al. (Bächlin et al., 2008) given in equation **(2)** was used to derive NO_2 concentrations from the dispersion of nitrogen oxides (NO_x) emissions related to road traffic. This mathematical function was initially built to retrieve NO_2 concentrations from NO_x concentration measurements. Its benefits in the purpose of micro-scale modeling of NO_2 concentrations in urban areas was recently demonstrated through CFD modeling (Reiminger et al., 2024) and AI modeling (Jurado et al., 2023).

$$[NO_2] = \frac{29.[NO_x]}{[NO_x] + 35} + 0.217\,[NO_x] \qquad (2)$$

where $[NO_2]$ and $[NO_x]$ are nitrogen dioxide and nitrogen oxides concentrations [g/m^3], respectively.

Then, NO_2 background concentrations available in the input data were added to the results of equation **(2)** to include external sources of this pollutant in the final result of modeling.

Lastly, the radiation model considered and used in this study for the non-neutral simulations corresponds to the *solarLoad* model included in the OpenFOAM library. In particular, this model requires the latitude, longitude, solar radiation, day of the year and time to be specified in order to calculate the position of the sun and the radiative heat flux induced on all the wall surfaces in the computational domain, which includes vertical facades, horizontal roofs, ground surfaces, and other infrastructure elements found in reality.

2.2.2. Solver validation

Validation under neutral boundary layer conditions

A transient isothermal CFD solver from OpenFOAM (*pimpleFoam*) using the same methodology as described in the previous section (URANS, RNG k-epsilon turbulence model, Bachlin's empirical function, etc.) was used in a prior work also carried out on Antwerp, Belgium (Reiminger et al., 2024). In this study, measurements from 73 NO_2 passive samplers deployed across an 800 × 800 m^2 area including street canyons of various aspect ratios, open areas, roads with high traffic volumes, and a built-up environment representative of typical North-West European cities, provided a robust dataset for validating the modeling approach. The results of this solver showed very good agreement between modeled and monitored NO_2 concentrations, leading to around 15% discrepancies and resulting in performance criteria ($FAC2$ = 1.0, MFB = 0.11, $NMSE$ = 0.03, R = 0.73, $Target$ = 0.91, with $FAC2$ the factor of modeled values within a factor of two of observations, MFB the Mean Fractional Bias, $NMSE$ the Normalized Mean Squared Error and R the Pearson correlation coefficient) largely satisfying ambient air quality model acceptance built for urban dispersion model evaluation (Hanna and Chang, 2012; Thunis et al., 2012). The equations of the performance criteria are given in Supplementary material **SM1**.

When comparing the results of the previously validated pimpleFoam solver to the non-isothermal solver employed in this work (*buoyantBoussinesqPimpleFoam*) under identical meteorological conditions, with thermal effects disabled and the same computational setup as in Reiminger et al. (2024), both solvers produced nearly identical outcomes. Across the entire computational domain, the maximum discrepancies between the two numerical solutions remained below 1%. Consequently, the *buoyantBoussinesqPimpleFoam* solver used in the present study can be considered validated under neutral boundary layer conditions.

Validation under unstable boundary layer conditions

The numerical model was compared against wind tunnel experimental data provided by (Cui et al., 2016) under non-neutral conditions. Their experimental setup consisted of a complex 3D configuration including two successive buildings of distinct heights, a pollutant emitted at the top of the upwind building, a room inside the downwind building opened by two windows as well as a heated ground surface between the two buildings to simulate a local heat source. Temperature (horizontal profile), velocity and pollutant concentration (vertical profiles) were available outdoor between the two buildings and velocity and pollutant concentrations (horizontal profile) were available indoor in the middle of the downwind building's room. A schematic representation of the numerical model used to replicate the experimental setup is given in the supplementary material **Figure SM2.1**, while comparison between experimental and modeled data are given in **Figure SM2.2** for the outdoor environment and **Figure SM2.3** for the indoor environment for a very unstable case leading to a Richardson number Ri of -1.22. The results are presented in a dimensionless form, as detailed in (Cui et al., 2016).

Very good agreements between experimental data and numerical model results are obtained outdoor, for all the parameters experimentally followed (temperature, wind speed and pollutant concentration), leading to around 15% of differences on the concentration field. The results of this comparison also satisfied ambient air quality model acceptance criteria with $FAC2 = 1.0$, $MFB = 0.12$, $NMSE = 0.02$, $R = 0.97$ and $Target = 0.38$. The same observations can be made for the indoor environment, where the results between the modeled and measured data (wind speed and pollutant concentration) are also very close (8 % of variation on the concentration field), with the exception of the wind velocities at the first two experimental points, which are highly overestimated by the numerical model. This overestimation is probably due to an insufficient evaluation of the airflow pattern at the constriction between the outside atmosphere and the upstream window.

Based on these results, the numerical model used in this study is considered validated, both outdoor and indoor, under unstable atmospheric conditions.

Validation of the solar radiation model

The validation presented in the previous section demonstrates that the model is able to properly reproduce the impact of the thermal effects induced by heated surfaces on both the airflow and the dispersion of air pollutants. A final validation step was nevertheless required to assess the performance of the radiative model in accurately predicting surface temperatures based on the position of the sun, the induced radiation and the surrounding obstacles. To do so, the experimental setup and results from (Idczak et al., 2010, 2007) have been used. Their experimental setup consisted of four lines of containers lined up in parallel and placed in an open area located in Guerville, France. They monitored reference wind (velocity and direction) and reference atmospheric conditions (ambient temperature, solar radiation, etc.) as well as the surface temperature of the middle containers' facades for different heights. Their experimental results were given for a sunny day (28 July 2004) and a cloudy day (12 October 2004).

The sunny day was hourly modeled using the *buoyantBoussinesqPimpleFoam* solver coupled with the solar radiative model, and the modeled surface temperature obtained are given in the supplementary materials **Figure SM3** for three different heights. According to the results, wall surface temperatures are very well reproduced by the numerical model for the whole day of 28 July 2004. An averaged deviation of 5.2 % when comparing modeled and measured surface temperatures is achieved, with an average deviation of 3.5 % during daytime and 7.2 % during nighttime. This slightly larger deviation at night could be partly attributed to nocturnal terrestrial radiation and to the residual heat stored within urban surfaces, which continue to release energy into the atmosphere even in the absence of solar radiation, depending on their thermal properties.

Based on these results, the coupling between the solar radiation model and the numerical model for reproducing surface temperatures from solar radiation was considered valid.

2.2.3. Computational domain and boundary conditions

All simulations correspond to fully 3D geometries obtained considering buildings and roads present in the area of interest during 2016. An insight of the obtained geometry is given in **Figure 2** with the red lines corresponding to roads where traffic-related emissions were available, thus considered in the numerical model.

The computational domain was substantially greater than the built-up area modeled to follow COST Action 732 guidelines (Franke et al., 2007) concerning distances between buildings and domain boundaries ($5H_{max}$ between buildings and inlet, outlet, lateral, and top boundaries, with H_{max} the height of the higher building).

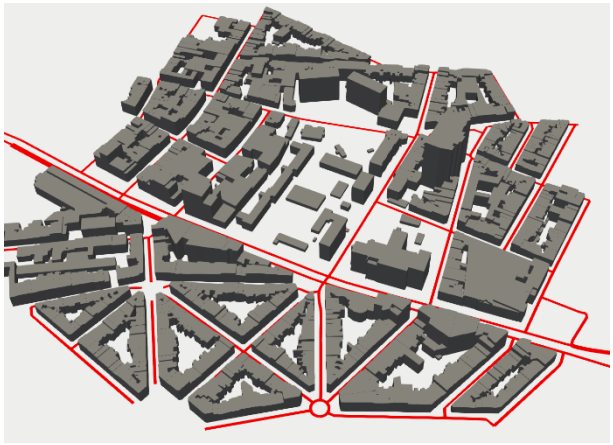

Figure 2. Overview of the 3D numerical model with red lines corresponding to roads for which emission data were available and modeled.

In this study, a mesh size of 1 meter was employed near wall boundaries, including the ground and buildings, with further refinement to 0.5 meters in proximity to pollutant sources. The meshes used in this study are unstructured and were generated with the *snappyHexMesh* utility provided in OpenFOAM v2306. With a domain size of 1 × 1 km^2, this approach resulted in a number of grid cells ranging between 8 and 10 million, depending on the specific scenario. This mesh size, which produces results insensitive to mesh size variations (Ioannidis et al., 2024; Santiago et al., 2019), was also previously used to validate the neutral version of the CFD model against 73 in-situ experimental concentration measurements (Reiminger et al., 2024). It is important to note that a 0.5-meter mesh size can be considered as relatively small for CFD modeling of air pollution in full-scale real urban environments. Indeed, mesh sizes in such studies are more commonly found to be around 1 meter (Sanchez et al., 2017; Vranckx et al., 2015) or larger, sometimes extending up to 2 meters (Martín et al., 2024).

Velocity profiles following eq. **(3)** and turbulence profiles following eq. **(4** and **5)** were specified at the inlet boundary following Richards and Norris (2011) recommendations, and a free-stream condition was applied at the outlet boundary to allow the flow to fully develop. No-slip conditions were set to all wall boundaries (ground and building faces and roofs) and symmetry conditions to the lateral and upper boundaries.

$$U = \frac{u_*}{\kappa} ln\left(\frac{z + z_0}{z_0}\right) \qquad (3)$$

$$k = \frac{{u_*}^2}{\sqrt{C_\mu}} \qquad (4)$$

$$\varepsilon = \frac{{u_*}^3}{\kappa . z} \qquad (5)$$

where U is the wind velocity [m.s^{-1}], k is the turbulent kinetic energy [m^2.s^{-2}], ε is the turbulence dissipation rate [m^2.s^{-3}], u_* is the friction velocity [m.s^{-1}], κ is the von Kármán constant [-] taken to 0.41, z is the altitude [m], z_0 is the roughness height [m] taken as 0.5 m to stand for built-up areas (Hahmann et al., 2015; Troen and Petersen, 1989) and C_μ is a CFD constant [-] taken as 0.085.

Emissivity (ε), thermal conductivity (κ) and thermal diffusivity (α) of the wall boundaries were set according to recommended values given in the literature (Bekkouche et al., 2016; Florides et al., 2002). The corresponding values are given in **Table 1**.

Table 1. Thermal properties of surface materials considered in the numerical model.

Type of surface	Ground surfaces	Wall surface
ε [-]	0.95	0.95
κ [$W.m^{-1}.K^{-1}$]	0.93	0.89
α [$m^2.s^{-1}$]	5.8×10^{-7}	5.6×10^{-7}

Traffic exhaust emissions were modeled using volumetric pollutant sources along the roads and over one mesh height (0.5 m), considering emissions of each road segment.

Lastly, simulations were performed using second order schemes for all divergent, gradients and Laplacians terms and were run until full convergence, leading to residuals under 10^{-5}.

2.2.4. Meteorological scenarios considered

A total of 12 hourly meteorological scenarios was modeled, each observed in Antwerp during the month of August 2016. These scenarios have been chosen to cover different wind speeds and directions, as well as solar radiation. The details of these scenarios and their corresponding Pasquill stability classes are given in **Table 2**. These classes, originally defined by Pasquill (1961), are an empirical classification of atmospheric turbulence conditions based on factors such as wind speed, solar radiation, and cloud cover. They range from highly unstable (class A) to stable (class F) conditions, reflecting how pollutants disperse in the lower atmosphere.

Table 2. Hourly meteorological scenarios modeled and their corresponding Pasquill stability classes.

Scenario	Date	Hour	Wind direction [°]	Wind velocity at 30 m [$m.s^{-1}$]	Ambient air temperature [°C]	Total solar radiation [$W.m^{-2}$]	Relative humidity [%]	Pasquill stability class*
S1	8/17/2016	1:00 PM	98	4.2	24.8	793	48	A-B
S2	8/18/2016	1:00 PM	118	2.1	23.5	736	51	A
S3	8/19/2016	7:00 AM	43	1.9	16.2	133	81	B
S4	8/19/2016	10:00 AM	19	1.8	22.0	310	65	B
S5	8/20/2016	2:00 PM	325	6.5	23.0	589	47	B-C
S6	8/21/2016	2:00 PM	279	4.9	19.5	509	76	B-C
S7	8/22/2016	11:00 AM	311	5.0	21.2	657	74	B-C
S8	8/23/2016	3:00 PM	38	2.5	29.3	606	44	A-B
S9	8/24/2016	2:00 PM	49	3.3	32.5	710	42	A-B
S10	8/24/2016	6:00 PM	70	3.6	31.7	176	39	C
S11	8/25/2016	7:00 AM	55	2.8	21.2	167	72	B
S12	8/28/2016	1:00 PM	287	6.1	24.8	663	53	B-C

* estimated based on wind velocity and total solar radiation according to (El-Ouartassy et al., 2022).

In this study, two comparison metrics are employed, namely the Relative Error (RE) as outlined in equation **(6)**, and the Normalized Absolute Error (NAE) detailed in equation **(7)**. While the first metric evaluates errors made by a numerical model in relation to observed data, the second metric facilitates a comparison of variations between two model outcomes without presupposing superiority of one over the other.

$$RE = \frac{|M - O|}{O} \qquad (6)$$

with M modeled concentration value and O the observed concentration value.

$$NAE = \frac{1}{N}\sum_{i=1}^{N}\frac{|M1_i - M2_i|}{(\overline{M1} + \overline{M2})/2} \qquad (7)$$

with N the number of data in the dataset, $M1_i$ (resp. $M2_i$) the i^{th} concentration value modeled by the first (resp. the second) numerical model and $\overline{M1}$ (resp. $\overline{M2}$) the concentration values modeled by the first (resp. second) numerical model averaged over the whole dataset.

3. Results

3.1. Qualitative comparison of the differences between neutral and non-neutral simulation outcomes

As a first step of comparison, results obtained using the neutral and non-neutral models were firstly compared qualitatively at human height (1.5 m).

Figure 3 illustrates the outcomes achieved using the two modeling approaches for a particularly warm day corresponding to scenario S9 (24 August 2016, 2:00 PM). According to **Figure 3 (B)**, and as a result of the wall heat flux induced by the solar radiation depicted in **Figure 3 (A)**, high overheating (i.e., temperature difference between isothermal and non-isothermal results) of around 10 K and up to 20 K can be observed in some areas. When juxtaposing these findings with the wind velocity magnitude and their corresponding vortices depicted in **Figure 3 (C1)**, it appears that heightened overheating predominantly occurs in regions characterized by air recirculation, and particularly at lower velocities. The relationship between air movements and temperatures is reciprocal, just as air movements influence temperatures, temperatures in turn influence air movements through turbulence. Indeed, upon comparing **Figure 3 (C1)** to **(C2)**, in other words, comparing the velocity results of the non-neutral and neutral models respectively, significant discrepancies can be observed: the non-neutral model leads to overall higher velocities in the whole area. This contrast is particularly noticeable in the central region of the area, where the non-neutral model shows velocities ranging from 3 to 5 m/s, while the neutral model indicates velocities ranging from 0 to 1 m/s. Additionally, recirculation patterns obtained by the two models are also different. As a consequence, since air pollutant dispersion is predominantly governed by convection and turbulent diffusion, there are also significant disparities in the NO_2 concentration maps which are observable when comparing **Figure 3 (D1)** and **(D2)**. Indeed, NO_2 concentration results from the non-neutral model generally exhibit lower values (29.9 µg/m^3 on average at 1.5 m height) compared with those from the neutral model (36.7 µg/m^3 on average at 1.5 m height). More specifically, at the bottom of the area, concentrations exceeding 80 µg/m^3 are frequently observed along the primary traffic artery and also at its intersection with the three southbound streets, whereas concentrations predicted by the non-neutral model at the same locations more commonly hover around 40 µg/m^3 or lower. Finally, it is noteworthy that the hotspots of NO_2 pollution modeled by the non-neutral and neutral models differ, with the latter tending to identify a greater number of hotspots.

Results from scenario S3 (19 August 2016, 7:00 AM) are additionally provided in **Figure 4**. This scenario is the extreme opposite from scenario S9 presenting distinct meteorological conditions characterized by significantly reduced solar radiation levels and lower solar elevation, resulting in an ambient air temperature twice as low. The input wind velocity for this scenario is approximately half that of the previous one, with no significant difference in wind direction. Consequently, and as depicted in **Figure 4 (A)**, the modeled wall heat flux is reduced by a factor of ten in this scenario compared to the previous scenario resulting in maximum overheating of 5 K, but more commonly observed overheating of 1 K as indicated in **Figure 4 (B)**. According to **Figure 4 (C1)** and **(C2)**, even such minor temperature fluctuations result in disparities between the wind velocities modeled by the neutral and non-neutral models, though to a significantly lesser degree than observed previously. Nonetheless, the recirculation patterns remain unchanged. Consequently, while still discernible, the discrepancies in NO_2 concentrations between the two models are less pronounced according to **Figure 4 (D1)** and **(D2)**. Lastly, the predicted hotspots of NO_2 concentrations remain consistent.

https://doi.org/10.1016/j.apr.2024.102383

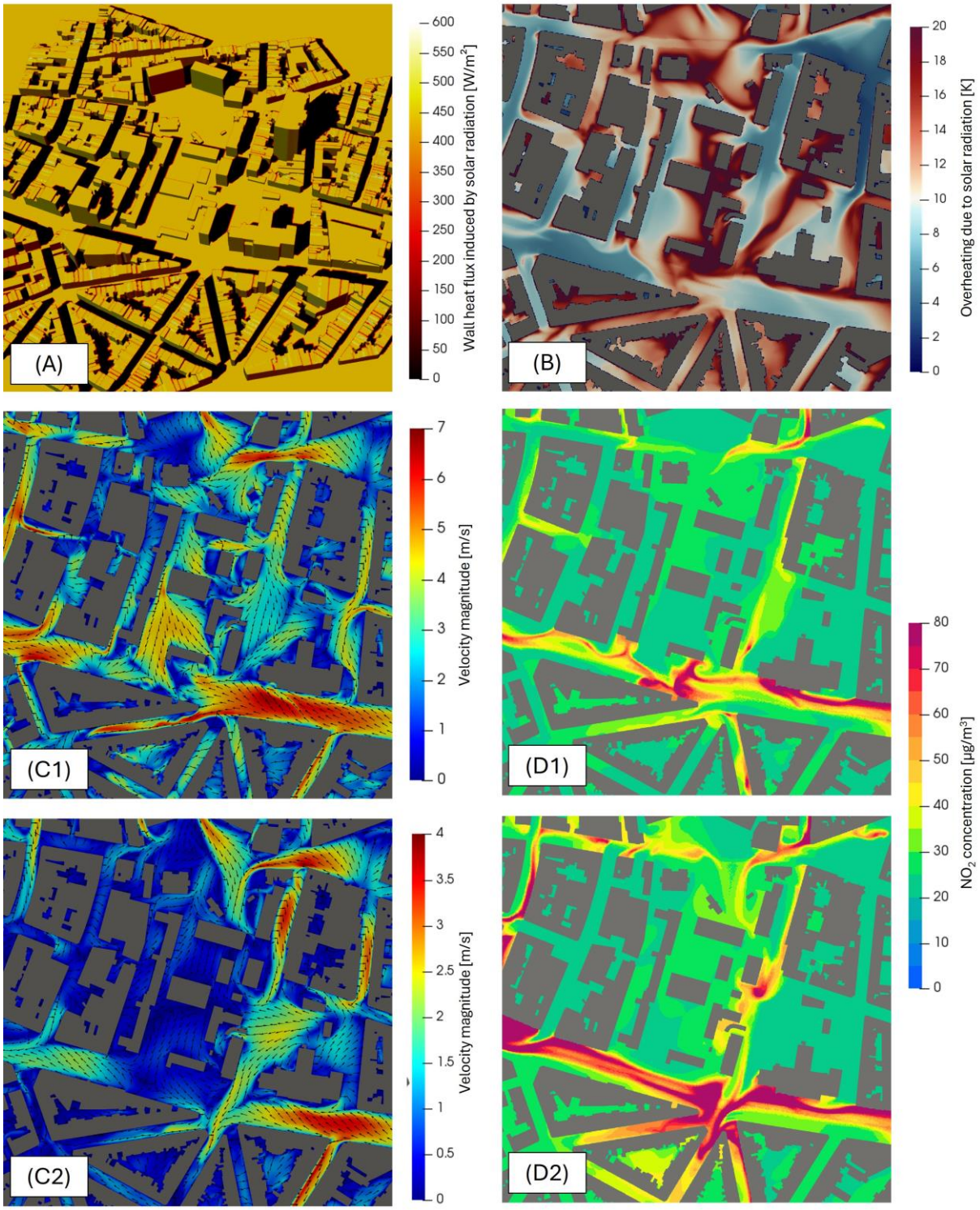

Figure 3. Numerical results for scenario S9 (24 August 2016, 2:00 PM) with **(A)** 3D wall heat flux (radiative model), **(B)** overheating at 1.5m height (non-neutral model), **(C1)** wind velocity at 1.5 m (non-neutral model), **(C2)** wind velocity at 1.5 m (neutral model), **(D1)** NO_2 concentration at 1.5 m (non-neutral model) and **(D2)** NO_2 concentration at 1.5 m (neutral model).

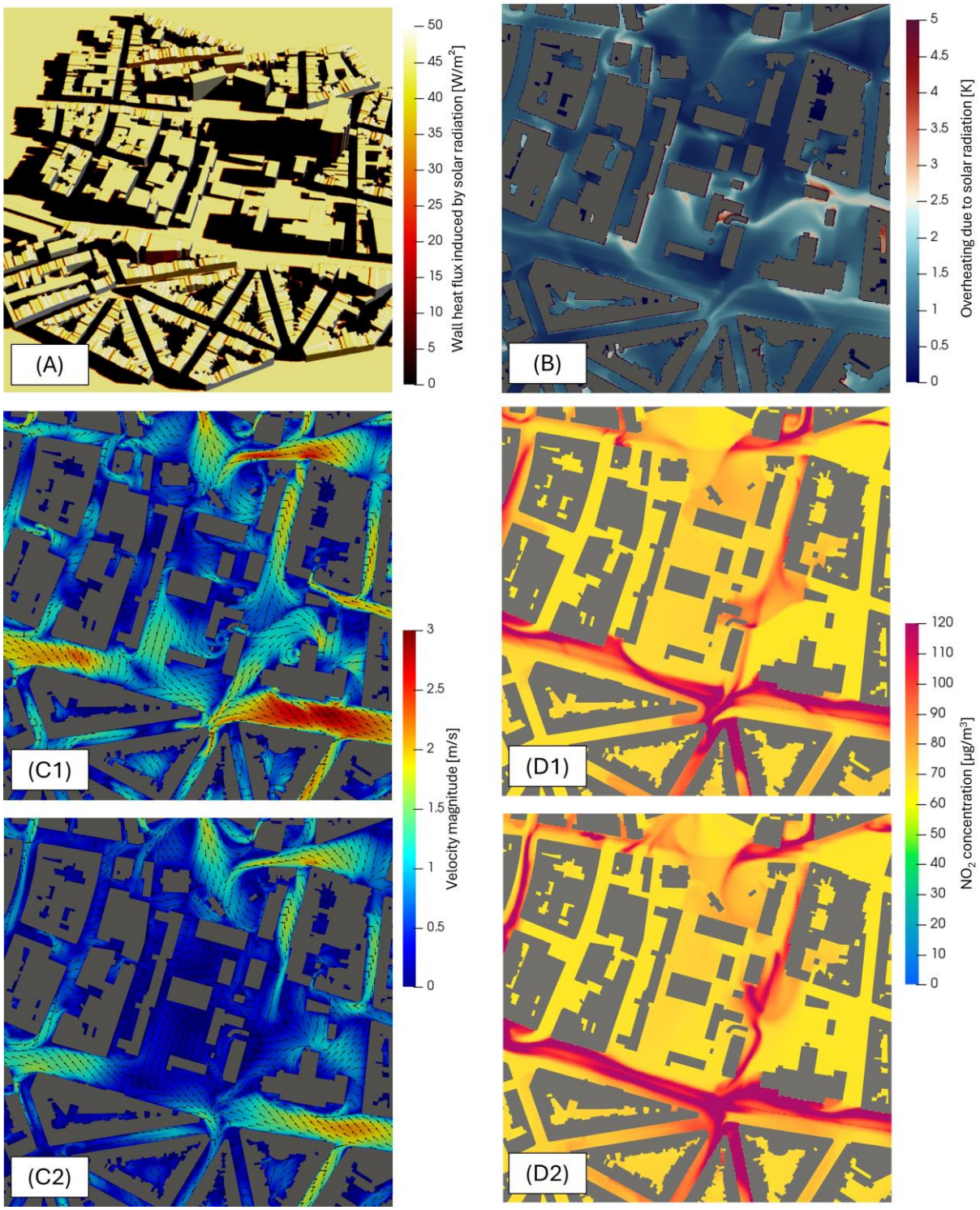

Figure 4. Numerical results for scenario S3 (19 August 2016, 7:00 AM) with **(A)** 3D wall heat flux (radiative model), **(B)** overheating at 1.5m height (non-neutral model), **(C1)** wind velocity at 1.5 m (non-neutral model), **(C2)** wind velocity at 1.5 m (neutral model), **(D1)** NO_2 concentration at 1.5 m (non-neutral model) and **(D2)** NO_2 concentration at 1.5 m (neutral model).

3.2. Quantitative comparison of the variations between modeled NO_2 concentrations

As a second step of comparison, variations between NO_2 concentrations modeled by the neutral and non-neutral models as a function of the scenario considered were assessed using the NAE metric. The corresponding results are gathered in **Table 3**.

Table 3. Normalized Absolute Errors (NAE) between neutral and non-neutral models depending on the scenario considered.

Scenario	S1	S2	S3	S4	S5	S6	S7	S8	S9	S10	S11	S12
NAE [%]	33%	32%	10%	17%	28%	30%	31%	29%	29%	10%	8%	32%

Based on these findings, significant discrepancies are evident between the two models, with NAEs ranging from 8% to 32% across the different modeled scenarios. Specifically, five scenarios exhibit $NAEs$ of 30% or more, while three scenarios display $NAEs$ of 10% or less, resulting in an average NAE of 24% across all the modeled scenarios (it is essential to note that the NAE metric stands for averaged variations which conceal greater disparities at specific spatial points, as discussed in the previous section). These differences in NAE results should be considered in light of the earlier observations. Indeed, high variations in modeled concentrations have been observed for scenario S9, leading to NAE = 29%, while lower variations were observed for scenario S3, leading to NAE = 10%. In addition, eight scenarios result in discrepancies exceeding 25 % (S1, S2, S5, S6, S7, S8, S9 and S12), while four scenarios yield discrepancies below 20 % (S3, S4, S10 and S11), with the majority of the latter under 10%. A comprehensive analysis of the underlying causes of these discrepancies is presented in Section 3.4.

Based on these results, the two numerical models lead therefore to significant differences in predicting hourly NO_2 concentration for all the meteorological conditions considered in this study.

3.3. Comparison of the modeled NO_2 concentrations with the air quality station data

Theoretically, the non-neutral model is expected to be more precise than the neutral model, as it accounts for the influence of thermal exchanges in the air on wind speed fields and, consequently, on concentration fields. To provide information on this subject, modeled NO_2 concentrations from both models were extracted at the location of the air quality (AQ) station for each simulated scenario. Errors between observed and modeled concentrations were then calculated using the relative error (RE) metric, with the results introduced in **Figure 5**. REs between observed concentrations and background concentrations are also depicted in this figure to emphasize the contribution of the numerical models compared to only considering background concentrations (i.e., hourly NO_2 concentrations obtained using the RIO model solely, see Section 2.1).

According to **Figure 5**, the non-neutral model consistently yields lower REs compared to only considering background concentrations. This observation does not hold for the neutral model, which, in some scenarios (S6 and S7), yields equivalent results to the background concentrations or slightly worse (scenario S5). When comparing the neutral and non-neutral models, the latter performs better in the majority of scenarios (S1, S3, S5, S6, S7, S9, S10, S11, S12), is equivalent to the neutral model, or, at least, not significantly different in two scenarios (S4 and S8), and performs worse in one scenario (S2).

Overall, REs range from 15% to 68% when only considering background concentrations, from 13% to 65% when using the neutral model, and from 6% to 67% when using the non-neutral model. While the maximal errors are of the same order of magnitude across all three cases, the non-neutral model achieves the lowest minimal error. On average, the non-neutral model outperforms the neutral model, which in turn outperforms the background concentration, with average REs of 21%, 40%, and 48%, respectively.

Lastly, it is noteworthy that for several scenarios (S1, S5, S7, S9 and S12), the non-neutral model outperforms the neutral one by at least a factor of two, and up to eight times better for scenario S12. With a defined error acceptability threshold of 50% in line with the European air quality directive for hourly air

quality modeling (EU, 2008), the non-neutral model experienced a single failure, whereas the neutral model encountered five failures, including the sole scenario failed by the non-neutral model.

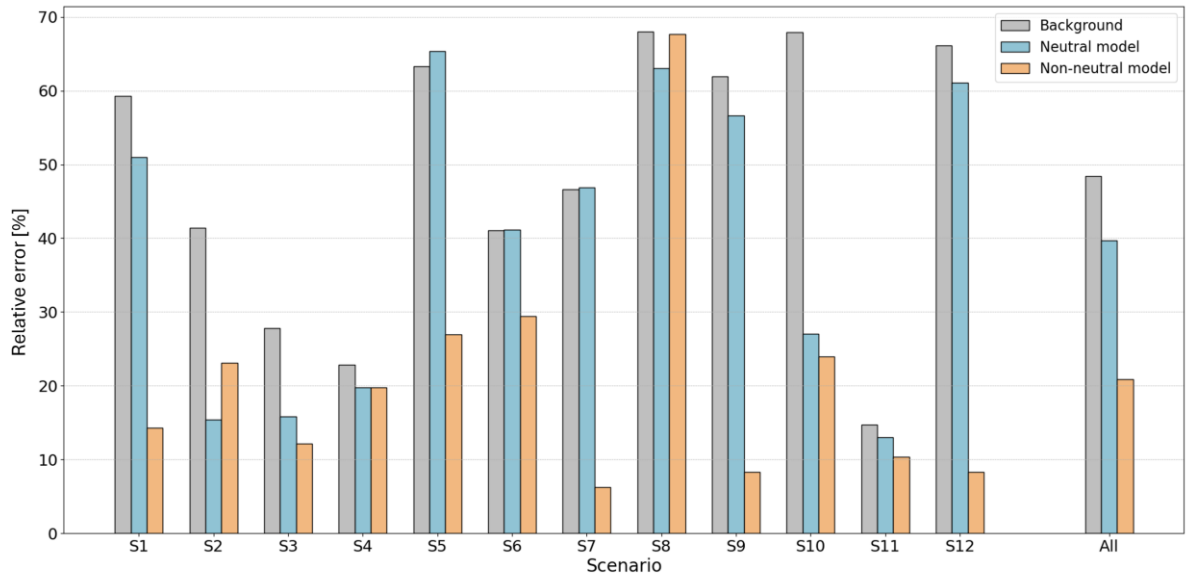

Figure 5. Comparison of Relative Errors (RE) between observed NO_2 concentrations at the air quality station and the predicted values from different models (background concentration alone, neutral model, and non-neutral model) depending on the meteorological scenario considered.

3.4. Scenarios clustering using unsupervised K-means machine learning

As a final analysis, the twelve meteorological scenarios considered in this study were analyzed to determine whether it was possible to explain why the non-neutral model performs very well in some scenarios while yielding equivalent results to the neutral one in others.

A straightforward comparison of the meteorological conditions for each scenario does not offer clear explanations. While the non-neutral model can perform well under both high and low solar radiation, wind velocities and directions, etc., indicating its versatility across various conditions, significant discrepancies also arise in results under similar meteorological conditions. Hence, an unsupervised clustering approach was employed to identify clusters of scenarios. The K-means algorithm was used for this purpose, considering all the parameters available in **Table 2**. Although parameters such as temperature, time of day, and atmospheric stability were initially also included, their influence on the clustering was less pronounced. This can be attributed to their indirect correlation with solar radiation and wind conditions, which ultimately emerged as the more dominant factors distinguishing the clusters. The results reveal the delineation of three clusters primarily influenced by solar radiation, wind velocity, and wind direction information. The results of the clustering based on these three variables are depicted in **Figure 6 (A)**, while **Figures 6 (B)**, **(C)**, and **(D)** present the projections onto each individual plane for enhanced clarity.

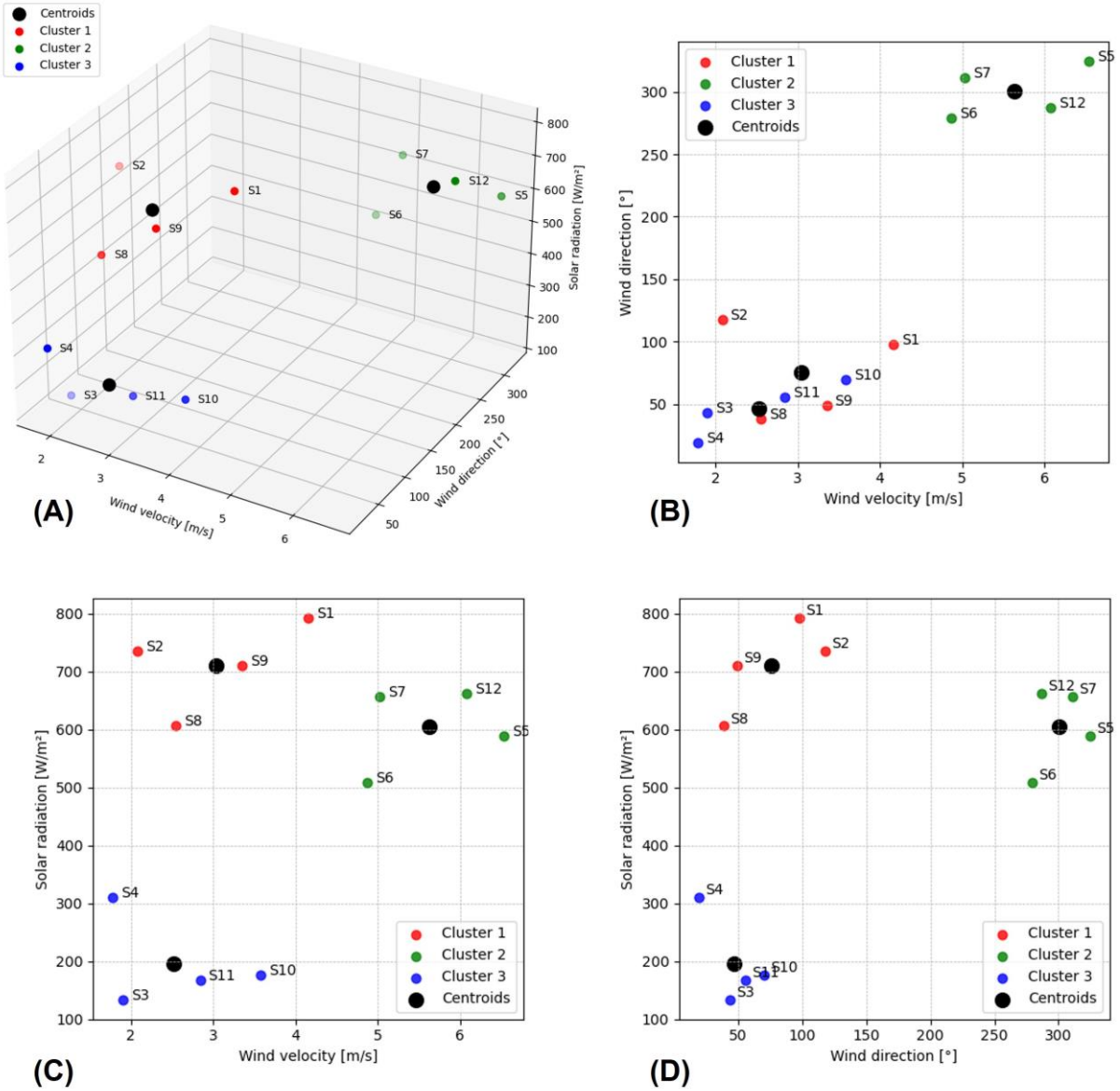

Figure 6. K-means clustering results with **(A)** 3D visualization of clusters based on wind velocity, wind direction, and solar radiation, **(B)** 2D view in the wind direction/wind velocity plane, **(C)** 2D view in the solar radiation/wind velocity plane, and **(D)** 2D view in the solar radiation/wind direction plane.

According to **Figure 6**, the three clusters of scenarios can be summarized as follows:

- Cluster 1: Characterized by low wind velocities (ranging from 2 to 4 m/s at 30 m height), high solar radiation (ranging from 600 to 800 W/m^2), and wind directions between 0 and 150°. The Pasquill stability classes of the included scenarios are A and A-B.

- Cluster 2: Defined by high wind velocities (ranging from 5 to 7 m/s at 30 m height), relatively high solar radiation (ranging from 500 to 700 W/m^2), and wind directions between 250° and 360°. The Pasquill stability classes of the included scenarios are B-C.

- Cluster 3: Identified by low wind velocities (ranging from 1 to 4 m/s at 30 m height), low solar radiation (ranging from 100 to 300 W/m^2), and wind directions between 0° and 100°. The Pasquill stability classes of the included scenarios are B and C.

With this new information, $NAEs$ and REs previously obtained were averaged based on the respective cluster of each scenario. The corresponding results are compiled in **Table 4**. These results provide some useful new information.

Table 4. Statistical parameters (NAE, RE, and factor of improvement) averaged across scenario clusters.

Cluster	Averaged NAE between neutral and non-neutral models [%]	$Avregaed\ RE$ compared to AQ station [%]			Factor of improvement using the non-neutral model [-]	
		Background concentration	Neutral model	Non-neutral model	Over background concentration	Over neutral model
1	31%	58%	47%	28%	2.1	1.7
2	30%	54%	54%	18%	3.0	3.0
3	11%	33%	19%	17%	1.9	1.1
All	24%	48%	40%	21%	2.3	1.9

Firstly, averaged $NAEs$ exhibit a similar order of magnitude between clusters 1 and 2 (around 30%) but are three times lower (11%) for cluster 3. This outcome is expected, as cluster 3 includes scenarios with low solar radiation, resulting in reduced thermal effects. Similar observations hold true for REs obtained by both the neutral and non-neutral models, yielding respective values of 19% and 17%.

When comparing REs between clusters 1 and 2, it becomes clear that the non-neutral model significantly outperforms the neutral model within cluster 2, while still demonstrating superiority within cluster 1 with a lesser extent. Indeed, as depicted in **Figure 5**, the non-neutral model consistently outperforms the neutral one across all four scenarios included in cluster 2 (scenarios S5, S6, S7, and S12). However, the situation is more varied within cluster 1, where the non-neutral model performs better for scenarios S1 and S9, but worse for scenarios S2 and S8.

As a final result indicated in **Table 4**, the mean factor of improvement by the non-neutral model over directly considering background concentration is 2.3, while it ranges from at least 1.1 (cluster 3) to up to 3.0 (cluster 2) over the neutral model. Across all scenarios considered, the factor of improvement achieved by the non-neutral model over the neutral model amounts to 1.9, proving its superiority in accurately modeling air pollution dispersion under unstable thermal conditions.

4. Discussion

According to the findings of this study, a non-isothermal, solar radiation-included CFD model yields more accurate results than a conventional isothermal CFD approach when modeling real hourly daytime meteorological scenarios under unstable atmospheric conditions. Recent research (Martín et al., 2024) has shown that using only neutral boundary layer conditions could provide good results for assessing long-term pollutant concentrations such as monthly concentrations. However, these results were obtained from only one full-scale experiment, and further evidence is needed to validate their broader applicability. Additionally, neglecting thermal effects and solar radiation in the model assumptions can lead to erroneous predictions of pollution hotspots and concentration levels for specific wind conditions. This statement should nonetheless be approached with caution. Although using a non-neutral model to simulate unstable hourly scenarios is expected to improve the prediction of long-term average concentrations, as indicated by this study's results, this type of model is more complex to parameterize and operate. Additionally, due to the inclusion of thermal effects induced by solar radiation, the known inverse relationship between the model's input velocity and resulting concentrations valid under a neutral boundary layer assumption (Reiminger et al., 2020), may not be maintained, particularly at low wind speeds where canopy turbulence is no longer dominated by shear turbulence. This may necessitate modeling multiple wind velocities and solar radiation scenarios for given wind directions, a requirement that is absent under neutral boundary layer conditions. Additionally, stable cases that were not assessed

in this study should also be considered. In particular, evaluating the maintenance and limits of stable boundary layer conditions when solar radiation is present would provide further insight into the interplay between thermal effects and turbulence. While stable stratification may initially reduce turbulent mixing, the introduction of solar radiation can modify vertical temperature profiles and influence buoyancy-driven flows. Determining the thresholds at which stable conditions break down or transition to other regimes would enhance our understanding of pollutant dispersion under varying atmospheric conditions. Furthermore, it is important to highlight that the comparison among the models evaluated in this study was constrained by the availability of data solely from a singular air quality measurement station operated by the Flemish Air Quality Agency. While this station provided valuable insights, the availability of additional data, especially with regards to spatialization, would have been optimal. This challenge is compounded by the inherent characteristics of such stations, which, due to their costly infrastructure, are limited in number and generally located far from each other, presenting an important obstacle for micro-scale model validation, especially CFD models, known for their resource-intensive nature in terms of both power and time. Consequently, it is recommended to replicate this research across diverse areas equipped with reliable and precise air quality measurement stations. Doing so would not only support the current findings but also shed light on the discrepancies observed between neutral and non-neutral models.

It is worth mentioning that certain phenomena, such as the influence of vegetation and traffic on wind velocity and turbulence at the road level, were not considered in this study. Including these factors, which have demonstrated their relevance in neutral cases, could be evaluated and compared with the current findings. This approach would help determine whether and to what extent the current results could be enhanced, especially in scenarios where the non-neutral model did not show significant improvements over the neutral one. This implies that other unaccounted phenomena may have influenced the results, highlighting the importance of identifying and understanding these factors to better comprehend the complexity behind the variations observed between neutral and non-neutral models.

Lastly, an aspect that warrants attention is the assumption of isotropic turbulent diffusion. Although this simplification is commonly made for computational convenience, it may not fully reflect the complexity of real-world flow dynamics, particularly under conditions influenced by solar radiation. Positive buoyancy effects can create vertical temperature gradients that, in turn, affect turbulence characteristics and potentially result in anisotropic pollutant dispersion. Such differences suggest that isotropic turbulence models might not fully capture the nuanced influence of buoyancy-driven flows. Future research could consider more advanced turbulence closure models or incorporate anisotropic diffusion terms to enhance the fidelity of urban air quality predictions.

5. Conclusion

This research aimed to evaluate the advantages of incorporating non-isothermal conditions and solar radiation into Computational Fluid Dynamics (CFD) models for air pollution dispersion in real urban environments. Twelve unstable hourly meteorological scenarios were modeled in a neighborhood of Antwerp, Belgium, using both a conventional neutral CFD approach and a non-isothermal approach that included solar radiation. Comparing the results of an enhanced solar radiation-included model with those of a conventional neutral model against in-field monitored data demonstrated the improved accuracy and insights provided by non-neutral CFD simulations. The main findings of this study are as follows:

(1) Variation spanning from 8% to 32% (24% on average) are observed between the NO_2 concentration maps generated by the neutral and non-neutral models, mostly due to variation in the modeled wind fields. These discrepancies are observed in both the identification of concentration hotspots and the prediction of concentration levels.

(2) Non-neutral solar radiation-included CFD model outperforms the neutral CFD model on 75% of the hourly meteorological scenarios assessed. On the remaining scenarios, only one slightly advantages the neutral model.

(3) Model errors, in comparison to air quality station data, range from 13% to 65% (averaging at 40%) for the neutral model and from 6% to 67% (averaging at 21%) for the non-neutral model. Overall, the non-neutral model demonstrates superior performance compared to the neutral model.

(4) Both models exhibit comparable performance in scenarios characterized by low wind speeds (< 4 m/s at 10m height) and low solar radiation (< 300 W/m^2). The non-neutral model nevertheless demonstrates superior performance overall, particularly in conditions of higher solar radiation and variable wind speeds.

Lastly, our results highlight that incorporating solar radiation into micro-scale CFD air quality modeling is beneficial, suggesting promising avenues for real-world urban applications.. The integration of solar radiation-included CFD simulations notably represents a significant advancement in urban air quality modeling, with potential implications for enhancing air quality management strategies and informing urban planning decisions. Further work could be pursued on this basis to consolidate the current results or advance them further by considering other complex phenomena encountered in urban environments, for instance focusing on the additional impact of vegetation or vehicle induced turbulence.

Acknowledgment

The authors express their profound gratitude to Dr. Stijn Janssen and Dr. Fernando Martin for granting them the opportunity to participate in the FAIRMODE initiative. The access they provided to the data from the Antwerp test case was instrumental in making this work possible.

CRediT authorship contribution statement

Nicolas Reiminger: Conceptualization, Software, Formal analysis, Validation, Supervision, Project administration, Writing - Original Draft. **Xavier Jurado**: Conceptualization, Formal analysis, Writing - Review & Editing. **Loïc Maurer**: Writing - Review & Editing. **José Vazquez**: Supervision. **Cédric Wemmert**: Supervision, Project administration, Writing - Review & Editing.

References

Agathokleous, E., Sicard, P., 2021. Editorial overview: Current and future challenges of air pollution. Current Opinion in Environmental Science and Health 21, 100246. https://doi.org/10.1016/j.coesh.2021.100246

Bächlin, W., Bösinger, R., Brandt, A., Schultz, T., 2008. Überprüfung des NO-NO2-Umwandlungsmodells für die Anwendung bei Immissionsprognosen für bodennahe Stickoxidfreisetzung. Reinhaltung der Luft 66, 154–157.

Badach, J., Wojnowski, W., Gębicki, J., 2023. Spatial aspects of urban air quality management: Estimating the impact of micro-scale urban form on pollution dispersion. Computers, Environment and Urban Systems 99, 101890. https://doi.org/10.1016/j.compenvurbsys.2022.101890

Baumann-Stanzer, K., Andronopoulos, S., Armand, P., Berbekar, E., Efthimiou, G., Fuka, V., Gariazzo, C., Gašparac, G., Harms, F., Hellsten, A., Jurčáková, K., Petrov, A., Rákai, A., Stenzel, S., Tavares, R., Tinarelli, G., Trini Castelli, S., 2015. COST ES1006 Model evaluation case studies: Approach and results.

Bekkouche, S.M.E.A., Benouaz, T., Kaoulal, R., Hamdani, M., Cherier, M.K., 2016. Improvement of thermo-aeraulic comfort with integrated solar wall system under Saharan climate. Renew. Energy Environ. Sustain. 1, 9. https://doi.org/10.1051/rees/2016009

Chen, G., Hang, J., Chen, L., Lin, Y., 2023. Comparison of uniform and non-uniform surface heating effects on in-canyon airflow and ventilation by CFD simulations and scaled outdoor experiments. Building and Environment 244, 110744. https://doi.org/10.1016/j.buildenv.2023.110744

Chen, H., Kwong, J.C., Copes, R., Tu, K., Villeneuve, P.J., van Donkelaar, A., Hystad, P., Martin, R.V., Murray, B.J., Jessiman, B., Wilton, A.S., Kopp, A., Burnett, R.T., 2017. Living near major roads and the incidence of dementia, Parkinson's disease, and multiple sclerosis: a population-based cohort study. The Lancet 389, 718–726. https://doi.org/10.1016/S0140-6736(16)32399-6

Choi, J., Hong, J., Hong, T., 2023. Analysis of the effect of dust barriers on particulate matter dispersion from a construction site using CFD simulation. Environmental Pollution 338, 122679. https://doi.org/10.1016/j.envpol.2023.122679

Cui, P.-Y., Li, Z., Tao, W.-Q., 2016. Buoyancy flows and pollutant dispersion through different scale urban areas: CFD simulations and wind-tunnel measurements. Building and Environment 104, 76–91. https://doi.org/10.1016/j.buildenv.2016.04.028

EEA, 2023. Europe's air quality status 2023. Briefing no. 05/2023. European Environment Agency. https://doi.org/10.2800/59526

El-Ouartassy, Y., Korsakissok, I., Plu, M., Connan, O., Descamps, L., Raynaud, L., 2022. Combining short-range dispersion simulations with fine-scale meteorological ensembles: probabilistic indicators and evaluation during a ^{85}Kr field campaign. Atmos. Chem. Phys. 22, 15793–15816. https://doi.org/10.5194/acp-22-15793-2022

EU, 2008. Directive 2008/50/EC of the european parliament and of the council of 21 May 2008 on ambient air quality and cleaner air for Europe, European Union.

Ferziger, J.H., Perić, M., 2002. Computational Methods for Fluid Dynamics. Springer, Berlin, Heidelberg. https://doi.org/10.1007/978-3-642-56026-2

Florides, G.A., Tassou, S.A., Kalogirou, S.A., Wrobel, L.C., 2002. Measures used to lower building energy consumption and their cost effectiveness. Applied Energy 73, 299–328. https://doi.org/10.1016/S0306-2619(02)00119-8

Franke, J., Hellsten, A., Schlünzen, H., Carissimo, B., 2007. Best practice guideline for the CFD simulation of flows in the urban environment. COST Action 732.

Ghobadi, P., Nasrollahi, N., 2021. Assessment of pollutant dispersion in deep street canyons under different source positions: Numerical simulation. Urban Climate 40, 101027. https://doi.org/10.1016/j.uclim.2021.101027

Guo, Y., Xiao, Q., Ling, C., Teng, M., Wang, P., Xiao, Z., Wu, C., 2023. The right tree for the right street canyons: An approach of tree species selection for mitigating air pollution. Building and Environment 245, 110886. https://doi.org/10.1016/j.buildenv.2023.110886

Hahmann, A., Lennard, C., Badger, J., Vincent, C., Kelly, M., Volker, P., Agent, B., Refslund, J., 2015. Mesoscale modeling for the Wind Atlas of South Africa (WASA) project. https://doi.org/10.13140/RG.2.1.3735.6887

Hang, J., Liang, J., Wang, X., Zhang, X., Wu, L., Shao, M., 2022. Investigation of O3–NOx–VOCs chemistry and pollutant dispersion in street canyons with various aspect ratios by CFD simulations. Building and Environment 226, 109667. https://doi.org/10.1016/j.buildenv.2022.109667

Hanna, S., Chang, J., 2012. Acceptance criteria for urban dispersion model evaluation. Meteorol Atmos Phys 116, 133–146. https://doi.org/10.1007/s00703-011-0177-1

Hooyberghs, H., De Craemer, S., Lefebvre, W., Vranckx, S., Maiheu, B., Trimpeneers, E., Vanpoucke, C., Janssen, S., Meysman, F.J.R., Fierens, F., 2022. Validation and optimization of the ATMO-Street air quality model chain by means of a large-scale citizen-science dataset. Atmospheric Environment 272, 118946. https://doi.org/10.1016/j.atmosenv.2022.118946

Idczak, M., Groleau, D., Mestayer, P., Rosant, J.-M., Sini, J.-F., 2010. An application of the thermo-radiative model SOLENE for the evaluation of street canyon energy balance. Building and Environment 45, 1262–1275. https://doi.org/10.1016/j.buildenv.2009.11.011

Idczak, M., Mestayer, P., Rosant, J.-M., Sini, J.-F., Violleau, M., 2007. Micrometeorological Measurements in a Street Canyon during the Joint ATREUS-PICADA Experiment. Boundary-Layer Meteorol 124, 25–41. https://doi.org/10.1007/s10546-006-9095-z

Ioannidis, G., Li, C., Tremper, P., Riedel, T., Ntziachristos, L., 2024. Application of CFD Modelling for Pollutant Dispersion at an Urban Traffic Hotspot. Atmosphere 15, 113. https://doi.org/10.3390/atmos15010113

Janssen, S., Dumont, G., Fierens, F., Mensink, C., 2008. Spatial interpolation of air pollution measurements using CORINE land cover data. Atmospheric Environment 42, 4884–4903. https://doi.org/10.1016/j.atmosenv.2008.02.043

Jurado, X., Reiminger, N., Maurer, L., Vazquez, J., Wemmert, C., 2023. Assessment of a deep learning model for monitoring atmospheric pollution: Case study in Antwerp, Belgium. Sustainable Cities and Society 99, 104951. https://doi.org/10.1016/j.scs.2023.104951

Kubilay, A., Derome, D., Carmeliet, J., 2018. Coupling of physical phenomena in urban microclimate: A model integrating air flow, wind-driven rain, radiation and transport in building materials. Urban Climate 24, 398–418. https://doi.org/10.1016/j.uclim.2017.04.012

Liu, S., Yang, X., Yang, H., Gao, P., Hang, J., Wang, Q., 2021. Numerical investigation of solar impacts on canyon vortices and its dynamical generation mechanism. Urban Climate 39, 100978. https://doi.org/10.1016/j.uclim.2021.100978

Manisalidis, I., Stavropoulou, E., Stavropoulos, A., Bezirtzoglou, E., 2020. Environmental and Health Impacts of Air Pollution: A Review. Front. Public Health 8, 14. https://doi.org/10.3389/fpubh.2020.00014

Martín, F., Janssen, S., Rodrigues, V., Sousa, J., Santiago, J.L., Rivas, E., Stocker, J., Jackson, R., Russo, F., Villani, M.G., Tinarelli, G., Barbero, D., José, R.S., Pérez-Camanyo, J.L., Santos, G.S., Bartzis, J., Sakellaris, I., Horváth, Z., Környei, L., Liszkai, B., Kovács, Á., Jurado, X., Reiminger, N., Thunis, P., Cuvelier, C., 2024. Using dispersion models at microscale to assess long-term air pollution in urban hot spots: A FAIRMODE joint intercomparison exercise for a case study in Antwerp. Science of The Total Environment 925, 171761. https://doi.org/10.1016/j.scitotenv.2024.171761

Ming, T., He, F., Wu, Y., Shi, T., Su, C., Wang, C., Li, Z., Chen, W., de Richter, R., 2023. The effect of noise barriers on viaducts on pollutant dispersion in complex street canyons. Energy and Built Environment 4, 589–600. https://doi.org/10.1016/j.enbenv.2022.05.003

O'Regan, A.C., Nyhan, M.M., 2023. Towards sustainable and net-zero cities: A review of environmental modelling and monitoring tools for optimizing emissions reduction strategies for improved air quality in urban areas. Environmental Research 231, 116242. https://doi.org/10.1016/j.envres.2023.116242

Pantusheva, M., Mitkov, R., Hristov, P.O., Petrova-Antonova, D., 2022. Air Pollution Dispersion Modelling in Urban Environment Using CFD: A Systematic Review. Atmosphere 13, 1640. https://doi.org/10.3390/atmos13101640

Pasquill, F., 1961. The Estimation of the Dispersion of Windborne Material. Meteorological Magazin 90, 33–49.

Reiminger, N., Jurado, X., Maurer, L., Vazquez, J., Wemmert, C., 2024. Modeling NO2 concentrations in real urban areas using computational fluid dynamics: A comparative analysis of methods to assess NO2 concentrations from NOx dispersion results. Sustainable Cities and Society 103, 105286. https://doi.org/10.1016/j.scs.2024.105286

Reiminger, N., Jurado, X., Vazquez, J., Wemmert, C., Blond, N., Dufresne, M., Wertel, J., 2020. Effects of wind speed and atmospheric stability on the air pollution reduction rate induced by noise barriers. Journal of Wind Engineering and Industrial Aerodynamics 200, 104160. https://doi.org/10.1016/j.jweia.2020.104160

Richards, P.J., Norris, S.E., 2011. Appropriate boundary conditions for computational wind engineering models revisited. Journal of Wind Engineering and Industrial Aerodynamics 99, 257–266. https://doi.org/10.1016/j.jweia.2010.12.008

Rodrigues, V., Gama, C., Ascenso, A., Oliveira, K., Coelho, S., Monteiro, A., Hayes, E., Lopes, M., 2021. Assessing air pollution in European cities to support a citizen centered approach to air quality management. Science of The Total Environment 799, 149311. https://doi.org/10.1016/j.scitotenv.2021.149311

Sanchez, B., Santiago, J.L., Martilli, A., Martin, F., Borge, R., Quaassdorff, C., de la Paz, D., 2017. Modelling NOX concentrations through CFD-RANS in an urban hot-spot using high resolution traffic

emissions and meteorology from a mesoscale model. Atmospheric Environment 163, 155–165. https://doi.org/10.1016/j.atmosenv.2017.05.022

Santiago, J., Rivas, E., Sanchez, B., Buccolieri, R., García Vivanco, M., Martilli, A., Martin, F., 2024. Impact of single and combined local air pollution mitigation measures in an urban environment. Science of The Total Environment 924, 171441. https://doi.org/10.1016/j.scitotenv.2024.171441

Santiago, J.-L., Buccolieri, R., Rivas, E., Sanchez, B., Martilli, A., Gatto, E., Martín, F., 2019. On the Impact of Trees on Ventilation in a Real Street in Pamplona, Spain. Atmosphere 10, 697. https://doi.org/10.3390/atmos10110697

Sin, C.H., Cui, P.-Y., Luo, Y., Jon, K.S., Huang, Y., 2023. CFD modeling on the canyon ventilation and pollutant exposure in asymmetric street canyons with continuity/discontinuity balconies. Atmospheric Pollution Research 14, 101641. https://doi.org/10.1016/j.apr.2022.101641

Thunis, P., 2018. On the validity of the incremental approach to estimate the impact of cities on air quality. Atmospheric Environment 173, 210–222. https://doi.org/10.1016/j.atmosenv.2017.11.012

Thunis, P., Georgieva, E., Pederzoli, A., 2012. A tool to evaluate air quality model performances in regulatory applications. Environmental Modelling & Software 38, 220–230. https://doi.org/10.1016/j.envsoft.2012.06.005

Tian, Y., Yao, X., Chen, L., 2019. Analysis of spatial and seasonal distributions of air pollutants by incorporating urban morphological characteristics. Computers, Environment and Urban Systems 75, 35–48. https://doi.org/10.1016/j.compenvurbsys.2019.01.003

Tominaga, Y., Stathopoulos, T., 2017. Steady and unsteady RANS simulations of pollutant dispersion around isolated cubical buildings: Effect of large-scale fluctuations on the concentration field. Journal of Wind Engineering and Industrial Aerodynamics 165, 23–33. https://doi.org/10.1016/j.jweia.2017.02.001

Toparlar, Y., Blocken, B., Maiheu, B., van Heijst, G.J.F., 2017. A review on the CFD analysis of urban microclimate. Renewable and Sustainable Energy Reviews 80, 1613–1640. https://doi.org/10.1016/j.rser.2017.05.248

Troen, I., Petersen, E.L., 1989. European wind atlas. Published for the Commission of the European Communities, Directorate-General for Science, Research, and Development, Brussels, Belgium by Risø National Laboratory, Roskilde, Denmark.

United Nations, 2019. World Urbanization Prospects: The 2018 Revision (ST/ESA/SER.A/420), Department of Economic and Social Affairs, Population Division. New York: United Nations.

Viana, M., de Leeuw, F., Bartonova, A., Castell, N., Ozturk, E., González Ortiz, A., 2020. Air quality mitigation in European cities: Status and challenges ahead. Environment International 143, 105907. https://doi.org/10.1016/j.envint.2020.105907

Vranckx, S., Vos, P., Maiheu, B., Janssen, S., 2015. Impact of trees on pollutant dispersion in street canyons: A numerical study of the annual average effects in Antwerp, Belgium. Science of The Total Environment 532, 474–483. https://doi.org/10.1016/j.scitotenv.2015.06.032

Wang, Y., Flageul, C., Maison, A., Carissimo, B., Sartelet, K., 2023. Impact of trees on gas concentrations and condensables in a 2-D street canyon using CFD coupled to chemistry modeling. Environmental Pollution 323, 121210. https://doi.org/10.1016/j.envpol.2023.121210

Zheng, X., Yang, J., 2022. Impact of moving traffic on pollutant transport in street canyons under perpendicular winds: A CFD analysis using large-eddy simulations. Sustainable Cities and Society 82, 103911. https://doi.org/10.1016/j.scs.2022.103911

Zheng, X., Yang, J., 2021. CFD simulations of wind flow and pollutant dispersion in a street canyon with traffic flow: Comparison between RANS and LES. Sustainable Cities and Society 75, 103307. https://doi.org/10.1016/j.scs.2021.103307